Journal of Biomedical Optics

BiomedicalOptics.SPIEDigitalLibrary.org

Comparison of magnetic resonance imaging-compatible optical detectors for in-magnet tissue spectroscopy: photodiodes versus silicon photomultipliers

Fadi El-Ghussein
Shudong Jiang
Brian W. Pogue
Keith D. Paulsen

SPIE.

Comparison of magnetic resonance imaging-compatible optical detectors for in-magnet tissue spectroscopy: photodiodes versus silicon photomultipliers

Fadi El-Ghussein, Shudong Jiang, Brian W. Pogue,* and Keith D. Paulsen
Dartmouth College, Thayer School of Engineering, Hanover, New Hampshire 03755, United States

Abstract. Tissue spectroscopy inside the magnetic resonance imaging (MRI) system adds a significant value by measuring fast vascular hemoglobin responses or completing spectroscopic identification of diagnostically relevant molecules. Advances in this type of spectroscopy instrumentation have largely focused on fiber coupling into and out of the MRI; however, nonmagnetic detectors can now be placed inside the scanner with signal amplification performed remotely to the high field environment for optimized light detection. In this study, the two possible detector options, such as silicon photodiodes (PD) and silicon photomultipliers (SiPM), were systematically examined for dynamic range and wavelength performance. Results show that PDs offer 10^8 (160 dB) dynamic range with sensitivity down to 1 pW, whereas SiPMs have 10^7 (140 dB) dynamic range and sensitivity down to 10 pW. A second major difference is the spectral sensitivity of the two detectors. Here, wavelengths in the 940 nm range are efficiently captured by PDs (but not SiPMs), likely making them the superior choice for broadband spectroscopy guided by MRI. © *The Authors. Published by SPIE under a Creative Commons Attribution 3.0 Unported License. Distribution or reproduction of this work in whole or in part requires full attribution of the original publication, including its DOI.* [DOI: 10.1117/1.JBO.19.7.070502]

Keywords: photodetectors; photodetection; magnetic resonance imaging; tomography; medical imaging; spectroscopy.

Paper 140259LR received Apr. 24, 2014; revised manuscript received Jun. 12, 2014; accepted for publication Jun. 16, 2014; published online Jul. 9, 2014.

Magnetic resonance imaging (MRI) tracts soft tissue structure and functional blood flow and vascular leakage in patients with high sensitivity to malignancy but with less to specificity. In recent years, significant interest has emerged to increase the specificity of the information by adding optical spectroscopy to the scanner, similar to the way positron emission tomography (PET) has been added to computed tomography and MRI systems.[1] The added value of optical spectroscopy would be in terms of the addition of molecular sensing, which is especially important in the understanding of newer biological therapies.[2] One of the major technical challenges in combining MRI with optical spectroscopy is signal detection over the wide dynamic range, which is required with a source-detection configuration that is compatible with routine clinical use.[3,4] The challenge is made even more demanding by the intense magnetic field that exists as well as the electromagnetic interference that occurs from the radiofrequency (RF) pulses involved. Special attention to system design is required in order to avoid performance degradation of either the MRI or diffuse optical tomography (DOT) imaging results. In this study, two promising detector designs, which offer a compact form factor with high dynamic range, were directly compared and their performance for tissue spectroscopy was evaluated.

The primary application under consideration in this evaluation is MRI-guided near-infrared spectroscopic tomography (NIRST) for breast imaging, which has been investigated in individual clinical trials and has shown value in terms of increasing the specificity of characterizing lesions.[4–6] The conceptual framework for this breast exam is to deploy the MRI scan for its anatomic and blood flow leakage (dynamic contrast) images, which are then used as prior information for NIRST quantification of total hemoglobin, oxygen saturation, water, and lipid contents.[7] Simultaneous MRI/DOT measurements enable datasets to be directly co-registered and analyzed. Essentially, all of the MR-compatible systems developed to date have relied on optical spectroscopy interfaces, which use long fiber optic cables to carry the light signal to and from the tissue of interest. Due to their bulk size, fragility, weight, and cost, the long fiber optic cables present a challenge to a system design that is clinically practical. A technological solution which places sources and detectors directly on the tissue and utilizes electrical (rather than optical) signal transfer on MRI compatible wires would be more desirable from a clinical perspective.

In order to investigate photon detectors that directly couple to tissue, MRI-compatible nonferromagnetic-based solid-state semiconductor photon detectors must be used. The challenge with these types of detectors is their packaging, frontend electronics, and module housing. Detector packaging and module housing may be custom ordered or machined to maintain MRI compatibility, leaving the frontend electronics to constitute the major obstacle due to their incompatibility with MRI. The frontend electronics are typically and directly connected to the detector. A potential solution, however, is to have the frontend electronics outside the MRI room. This approach would minimize the footprint of the patient interface while keeping the system design simple and modular. A configuration where the amplifier electronics is kept outside the MR field limits the detectors of choice to photodiode (PDs) and silicon photomultiplier (SiPM) detectors. The aim of this study is to report on the performance of MRI compatible PDs and SiPMs when placed inside the scanner bore while being connected via an electrical cable to frontend electronics located outside the MRI room.

The usable dynamic range of the SiPM and PD detectors was measured inside the MRI bore while they were tethered to an optimized amplifier circuit located outside the MRI room at the distal end of a transmission line. An 8-m cable was used to connect the detectors to the preamplifiers through a conduit in the MRI room wall as shown in Fig. 1(a). The effect of the

*Address all correspondence to: Brian W. Pogue, E-mail: brian.pogue@dartmouth.edu

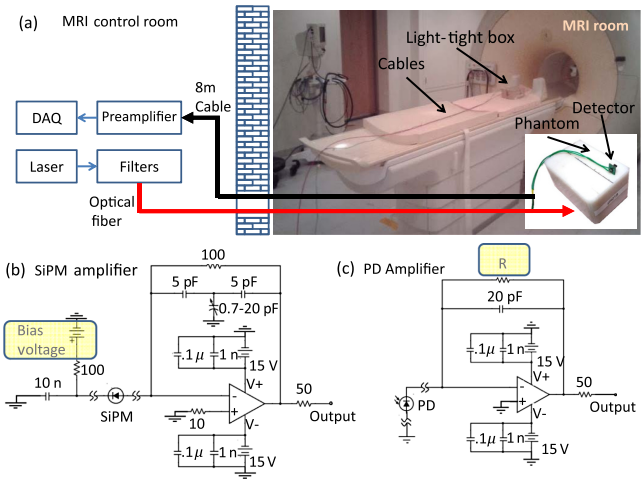

Fig. 1 Illustration of the source-detector electronics with coupling into the MRI. (a) Electrical schematics of the optimized amplifier circuits used at the distal end of the cables to the SiPM (b) and PD (c) detectors are shown.

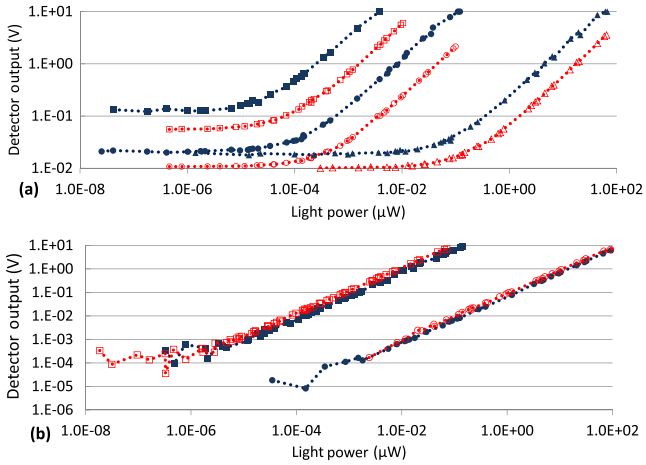

Fig. 2 In (a) the response of the SiPM detector at different bias voltages: 28 V (triangles), 28.5 V (circles), and 30.5 V (squares). The solid (blue) symbols denote the 661 nm wavelength response while the open (red) denote 948 nm. In (b) the response of the PD detector is shown using different amplifications, by varying the feedback resistance. Low gain was produced with feedback of 100 K Ω (circles) and high gain at a feedback of 100 M Ω (squares).

long separation between the detector and the frontend electronics was evaluated by comparing the dynamic range of the detectors when connected directly to the frontend electronics relative to when connected through a long electrical cable. The detectors were placed inside a light-tight box which had a small window that enabled laser light to enter. A fiber optic cable was used to deliver a continuous wave (CW) laser light to the detectors inside the MRI bore. Two different CW laser sources (661 and 948 nm) were used to compare the effects of wavelength on the detectors. Different neutral density filters were placed in front of the laser source in order to attenuate the laser light. The detector output at each filter setting was recorded with a 16-bit 100 KS/s PCI-6031E (National Instruments, Austin, Texas) data acquisition card. Phantom experiments were also performed in order to evaluate the performance of the detectors inside the MRI more fully. MRI scans of a silicon phantom with and without detectors mounted on top were acquired to investigate effects on the MRI image quality. Finally, data were acquired from the detectors while simultaneously running a MRI scan in order to identify the possible interference effects from the MRI RF pulses.

The SiPM detector used in this study was a 3×3 mm^2 MRI-compatible sensor from AdvansID (Povo, Trento, Italy) (ASD-RGB3S-P-50) with 3600 cells and a cell size of 50×50 μm^2 with a 45% fill factor. The SiPM detector was mounted on a surface mount to pin converter socket (ASD-EP-S-3) to simplify prototyping. The photodiode detector was a PIN type photodiode from Hamamatsu Inc. (Japan) (S5107-1369) with a 10×10 mm^2 active area. The detector was custom ordered to ensure MRI compatibility.

The SiPM detector was connected as shown in Fig. 1(b). A variable power supply was used to bias the SiPM detector through a 100 Ω resistor at several bias voltages: 28 to 30.5 V in 0.5 V increments. A transimpedance ultralow noise amplifier (AD797 Analog Devices, Norwood, Massachusetts) was used to amplify the detector's output signal.

The photodiode detector was operated in a zero-bias configuration for excellent linearity and low dark current as shown in Fig. 1(c). A low noise transimpedance amplifier (OPA827) was used to amplify the output signal. The gain of the amplifier circuit was set by using different feedback resistor values: 10 K, 100 K, 1 M, 10 M, 100 M, and 1 G Ω. The laser power was measured via a calibrated Hamamatsu power meter. Both amplifier designs were chosen after a range of possible designs were evaluated and their minimum sensitivity was measured.

The dynamic range as a function of incident light power for the SiPM is shown in Fig. 2(a) for a 661-nm laser (blue markers) and a 948-nm laser (red markers). Three different bias voltages are shown: 28 (triangles), 28.5 (circles), and 30.5 V (squares). Depending on the bias voltage, the dynamic range extends from ~10 pW to ~100 μW giving a total of 10^7 dynamic range (140 dB). Tethering the detector to the amplifier circuit did not affect the minimum sensitivity or dynamic range of the SiPM detector. The dynamic range for the photodiode detector is shown in Fig. 2(b). Two wavelengths are shown: 661 (blue) and 948 nm (red). The dynamic range of the setup depends on the gain of the amplifier circuit and extends from ~1 pW to ~100 μW giving a total of 10^8 dynamic range (160 dB). The circles in Fig. 2(b) represent a feedback resistor gain of 100 K Ω while the squares show data for a feedback resistor gain of 100 M Ω. The dynamic range results of the detectors tethered via the 8-m cable match the results of the detector directly coupled to the amplifiers for all feedback resistor gain values up to 100 M Ω. While higher gain reduces the frequency response of the amplifier, switching between different gains does not affect the measurements.

The detectors were used to measure the attenuation of the laser light as it penetrates a rectangular silicon phantom that simulates an optically dense breast. The laser light was incident on the bottom surface of the phantom and the photon detectors were placed one-at-a time on the top surface of the silicon phantom at nine different source-to-detector distances as shown in Fig. 3. The signal level depends on the laser power as well as the optical density of the phantom/tissue. Measurements using a PMT detector from our current MR-compatible system, which uses 12-m fiber optic cables to carry the light signal from the

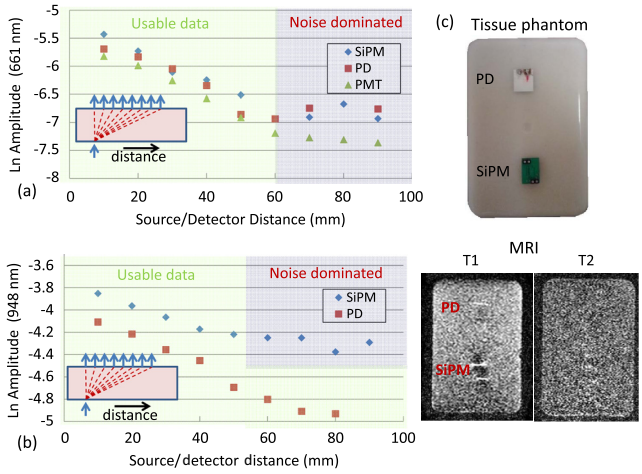

Fig. 3 Tissue phantom measurements using the PD, SiPM, and a fiber-optic coupled PMT for the 661 nm laser (a) and PD and SiPM for the 948 nm laser (b). Note the PMT used cannot detect light at 948 nm, hence was not included. Photo (top) and MRI scan (bottom) of the detectors mounted on the silicon phantom is also shown (c).

phantom to the detector, were acquired. The results using the PD, SiPM, and PMT detectors for 661-nm laser light are shown in Fig. 3(a). Figure 3(b) shows the attenuation of the 948-nm laser light as a function of distance for the PD and SiPM detectors. Although Fig. 3(a) is dominated by noise for source/detector distance over 60 mm, a breast imaging system utilizing such detectors can gently compress the breast with a setup similar to the breast interface described by Mastanduno et al.,[7] such that source/detector distances are within 60 mm.

A T1 MRI sequence with detectors mounted on the phantom showed minor artifacts for the SiPM detector, whereas a T2 sequence showed no obvious artifacts as shown in Fig. 3(c). These artifacts are attributed to the SiPM surface mount to pin converter socket in which the detector was mounted. It is possible to eliminate these artifacts by using an MRI-compatible converter. The detectors were also tested while concurrently performing an MRI scan where the RF pulses generated induced electromagnetic interference in the electrical cable leading to the preamplifier circuit causing saturation of the output signal. While it may not be feasible to completely shield the electrical cables, it is possible to synchronize MR acquisition with optical detection in order to avoid RF effects or to collect the optical data before or after the MRI scan while the patient has not moved in order to coregister MRI and optical results.

This study focused on the feasibility of using PDs and SiPMs inside the MRI bore for the development of a hybrid MRI/DOT system that efficiently and cost effectively covers the tissue of interest with an easily adaptable profile. The sensitivity limits of both detectors were found to be essentially identical if one were to consider the size of each sensor. The SiPM, however, is less sensitive to longer wavelengths; a feature that is unfortunate for applications where spectroscopy of water or lipids may be valuable. The PD has higher sensitivity at longer wavelengths, which is ideal for the recovery of water and lipids with DOT, since the spectral features of these absorbers are more prominent at longer wavelengths. Cable length did not affect the sensitivity or dynamic range of the SiPM measurements which agree with an earlier study by Kang et al[8] investigating photon counting behavior (energy resolution and timing) of the detector which is explained, in part, by the operational behavior of the SiPM detector where each photon generates an avalanche of electrons that can be easily identified and measured, and by the high impedance cables used. For the PD detector, the cable used for tethering did not affect the sensitivity and dynamic range for feedback resistor gain below 100 MΩ.

Acknowledgments

This work has been funded by NCI research grants R01 CA069544, R01CA176086, and R01 CA109558.

References

1. A. W. Sauter et al., "Combined PET/MRI: one step further in multimodality imaging," *Trends Mol. Med.* **16**(11), 508–15 (2010).
2. A. J. de Langen et al., "Monitoring response to antiangiogenic therapy in non-small cell lung cancer using imaging markers derived from PET and dynamic contrast-enhanced MRI," *J. Nucl. Med.* **52**(1), 48–55 (2010).
3. F. El-Ghussein et al., "Hybrid photomultiplier tube and photodiode parallel detection array for wideband optical spectroscopy of the breast guided by magnetic resonance imaging," *J. Biomed. Opt.* **19**(1), 011010 (2014).
4. V. Ntziachristos et al., "Concurrent MRI and diffuse optical tomography of breast after indocyanine green enhancement," *Proc. Natl. Acad. Sci. USA* **97**(6), 2767–2772 (2000).
5. C. M. Carpenter et al., "Image-guided optical spectroscopy provides molecular-specific information in vivo: MRI-guided spectroscopy of breast cancer hemoglobin, water, and scatterer size," *Opt. Lett.* **32**(8), 933–935 (2007).
6. M. A. Mastanduno et al., "Adaptable near-infrared spectroscopy fiber array for improved coupling to different breast sizes during clinical MRI," *Acad. Radiol.* **21**(2), 141–150 (2014).
7. B. W. Pogue et al., "Implicit and explicit prior information in near-infrared spectral imaging: accuracy, quantification and diagnostic value," *Philos. Transact. A Math. Phys. Eng. Sci.* **369**(1955), 4531–4557 (2011).
8. J. Kang et al., "A feasibility study of photosensor charge signal transmission to preamplifier using long cable for development of hybrid PET-MRI," *Med. Phys.* **37**(11), 5655–5664 (2010).